Multi-task Bayesian Compressive Sensing Method for Imaging Sparse Metallic Cylinders

L. Poli, G. Oliveri, A. Massa

Abstract

In this report, an innovative method for the localization of multiple sparse metallic targets is proposed. Starting from the local shape function formulation of the inverse scattering problem and exploiting the multitask Bayesian compressive sensing paradigm, a two-step approach is applied where, after a first estimation of the LSF scattering amplitudes, the reconstruction of the metallic objects is yielded through a thresholding and voting step. The calibration of the BCS parameters together with some preliminary results dealing with small scatterers reported.

1 Mathematical Formulation

1.1 MT-BCS-based PEC retrieval technique

Let us consider an investigation domain of extension D illuminated by a set of V known incident transverse-magnetic waves. Inside the investigation domain are placed one or more PEC objects, identified by a local shape function:

$$\gamma_n = \begin{cases} 1, & r_n \in \Theta_s \\ 0, & r_n \notin \Theta_s \end{cases} \quad (n = 1, ..., N)$$

where N is the number of cells in the investigation domain and Θ_s is the domain of the cylindrical conducting scatterer. Given the field scattered $E_v^{scatt}(x, y)$ from a a PEC cylinder, the data equation is defined

$$E_v^{scatt}(x, y) = \int_D J_v(x', y') G_{2D}(x, y/x', y') dx' dy' \tag{1}$$

where $E_v^{scatt}(x, y)$ is the scattered field, $G_{2D}^{ext}(x, y/x', y')$ is the two-dimensional free-space Green's function, and $J_v(x', y')$ is the contrast source.

In matricial form we have

$$[E_v^{scatt}] = [G_{2D}^{ext}][J_v] \tag{2}$$

where

$$[E_v^{scatt}] = \begin{bmatrix} E_v^{scatt}(x_1, y_1) \\ ... \\ E_v^{scatt}(x_m, y_m) \\ ... \\ E_v^{scatt}(x_M, y_M) \end{bmatrix} \tag{3}$$

with size $M \times 1$, $m = 1, ..., M$ and $v = 1, ..., V$, where M is the number of measurement points and V is the number of views;

$$[G_{2D}^{ext}] = \begin{bmatrix} G_{2D}^{ext}(\rho_{11}) & ... & G_{2D}^{ext}(\rho_{1n}) & ... & G_{2D}^{ext}(\rho_{1N}) \\ ... & ... & ... & ... & ... \\ G_{2D}^{ext}(\rho_{m1}) & ... & G_{2D}^{ext}(\rho_{mn}) & ... & G_{2D}^{ext}(\rho_{mN}) \\ ... & ... & ... & ... & ... \\ G_{2D}^{ext}(\rho_{M1}) & ... & G_{2D}^{ext}(\rho_{Mn}) & ... & G_{2D}^{ext}(\rho_{MN}) \end{bmatrix} \tag{4}$$

with size $M \times N$ where and $\rho_{mn} = \sqrt{\left[(x_m - x'_n)^2 + (y_m - y'_n)^2\right]}$.

$$[J_v] = \begin{bmatrix} J_v(x_1, y_1) \\ ... \\ J_v(x_n, y_n) \\ ... \\ J_v(x_N, y_N) \end{bmatrix} \tag{5}$$

with size $N \times 1$.

Using Compressive Sampling techniques it is possible to solve linear problems such as: given $\overline{y} = \overline{A} \cdot \overline{x}$ find $\overline{x}$ such that $\overline{x} \in C^M$ and $\overline{x}$ is sparse. We apply the multi-task bayesian compressive sampling technique (MT-BCS) to exploit the correlation between V problems defined through the data equation:

$$\begin{cases} E_1^{scatt}(x, y) = \int_D J_1(x', y') G_{2D}(x, y/x', y') dx' dy' \\ ... \\ E_v^{scatt}(x, y) = \int_D J_v(x', y') G_{2D}(x, y/x', y') dx' dy' \\ ... \\ E_V^{scatt}(x, y) = \int_D J_V(x', y') G_{2D}(x, y/x', y') dx' dy' \end{cases} \tag{6}$$

By expressing the formulation in matricial form, we have

$$\left\{ \begin{array}{c} [E_1^{scatt}] = [G_{2D}^{ext}][J_1] \\ ... \\ E_v^{scatt}] = [G_{2D}^{ext}][J_v] \\ ... \\ [E_V^{scatt}] = [G_{2D}^{ext}][J_V] \end{array} \right. \tag{7}$$

where

$$[E_v^{scatt}] = \left[\begin{array}{c} E_v^{scatt}(x_1, y_1) \\ ... \\ E_v^{scatt}(x_m, y_m) \\ ... \\ E_v^{scatt}(x_M, y_M) \end{array} \right] \tag{8}$$

with size $M \times 1$,

$$[G_{2D}^{ext}] = \left[\begin{array}{ccccc} G_{2D}^{ext}(\rho_{11}) & ... & G_{2D}^{ext}(\rho_{1n}) & ... & G_{2D}^{ext}(\rho_{1N}) \\ ... & ... & ... & ... & ... \\ G_{2D}^{ext}(\rho_{m1}) & ... & G_{2D}^{ext}(\rho_{mn}) & ... & G_{2D}^{ext}(\rho_{mN}) \\ ... & ... & ... & ... & ... \\ G_{2D}^{ext}(\rho_{M1}) & ... & G_{2D}^{ext}(\rho_{Mn}) & ... & G_{2D}^{ext}(\rho_{MN}) \end{array} \right] \tag{9}$$

with size $M \times N$,

$$[J_v] = \left[\begin{array}{c} J_v(x_1, y_1) \\ ... \\ J_v(x_n, y_n) \\ ... \\ J_v(x_N, y_N) \end{array} \right] \tag{10}$$

with size $N \times 1$.

For each view $v = 1, ..., V$ we estimate now the local shape function associated with the v-th view γ_n^v by using:

$$\gamma_n^v = \left\{ \begin{array}{ll} 1, & if\ J_v(x_n, y_n) \geq \eta Max_n \{J_v(x_n, y_n)\} \\ 0, & if\ J_v(x_n, y_n) < \eta Max_n \{J_v(x_n, y_n)\} \end{array} \right. \quad (n = 1, ..., N) \tag{11}$$

where η is suitably defined threshold (determined through calibration).

Finally, the local shape function is estimated as

$$\gamma_n = \left\{ \begin{array}{ll} 1, & if\ \sum_{v=1}^{V} J_v(x_n, y_n)/V \geq 0.5 \\ 0, & if\ \sum_{v=1}^{V} J_v(x_n, y_n)/V < 0.5 \end{array} \right. \quad (n = 1, ..., N) \tag{12}$$

2 Calibration

2.1 Multiple Cylinders $l = 0.16\lambda$

Goal: calibrate the $MT - BCS$ when dealing with a sparse scatterers

- Number of Views: V
- Number of Measurements: M
- Number of Cells for the Inversion: N
- Number of Cells for the Direct solver: D
- Side of the investigation domain: L

Test Case Description

Direct solver:

- Square domain divided in $\sqrt{D} \times \sqrt{D}$ cells
- Domain side: $L = 3\lambda$
- $D = 1296$ (discretization for the direct solver: $< \lambda/10$)

Investigation domain:

- Square domain divided in $\sqrt{N} \times \sqrt{N}$ cells
- $L = 3\lambda$
- $2ka = 2 \times \frac{2\pi}{\lambda} \times \frac{L\sqrt{2}}{2} = 6\pi\sqrt{2} = 26.65$
- $\#DOF = \frac{(2ka)^2}{2} = \frac{(2\times\frac{2\pi}{\lambda}\times\frac{L\sqrt{2}}{2})^2}{2} = 4\pi^2\left(\frac{L}{\lambda}\right)^2 = 4\pi^2 \times 9 \approx 355.3$
- N scelto in modo da essere vicino a $\#DOF$: $N = 324$ (18×18)

Measurement domain:

- Measurement points taken on a circle of radius $\rho = 3\lambda$
- Full-aspect measurements
- $M \approx 2ka \rightarrow M = 27$

Sources:

- Plane waves
- $V \approx 2ka \rightarrow V = 27$
- Amplitude: $A = 1$
- Frequency: 300 MHz ($\lambda = 1$)

PEC Object:

- $S = 10$ sparse square cylinders of side $\frac{\lambda}{6} = 0.1667$

MT-BCS parameters:

- Gamma prior on noise variance parameter: $a \in \left\{1 \times 10^0, 2 \times 10^0, 5 \times 10^0, 1 \times 10^{+1}, 2 \times 10^{+1}, 5 \times 10^{+1}, 1 \times 10^{+2}, 2 \times 10^{+2}, 5 \times 10^{+2}, 1 \times 10^{+3}, 2 \times 10^{+3}, 5 \times 10^{+3}, 1 \times 10^{+4}\right\}$
- Gamma prior on noise variance parameter: $b \in \left\{1 \times 10^{+0}, 5 \times 10^{-1}, 2 \times 10^{-1}, 1 \times 10^{-1}, 5 \times 10^{-2}, 2 \times 10^{-2}\, 1 \times 10^{-2}, 5 \times 10^{-3}, 2 \times 10^{-3}, 1 \times 10^{-3}, 5 \times 10^{-4}, 2 \times 10^{-4}, 1 \times 10^{-4}\right\}$
- Convergenze parameter: $\tau = 1.0 \times 10^{-8}$

Error Figures: Calibration

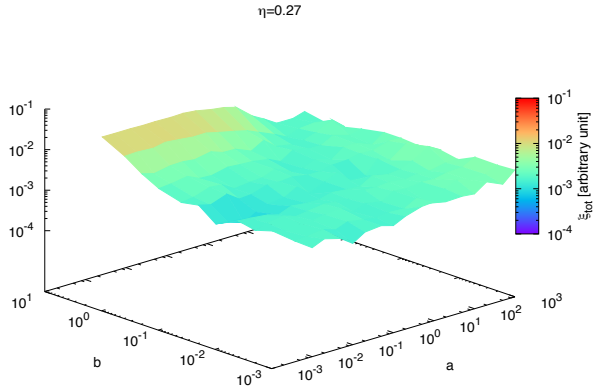

(a)

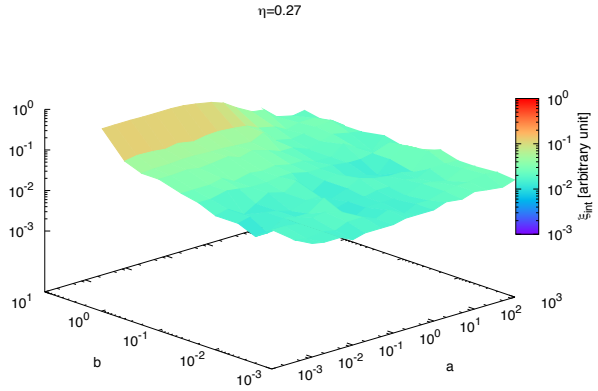

(b)

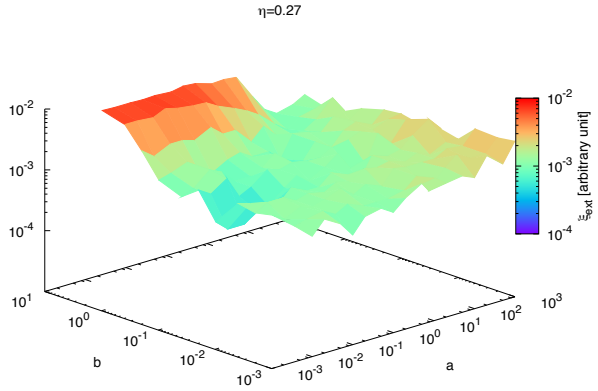

(c)

Figure 1. Behaviour of error figures as a function of the MT-BCS parameters a and b: (a) total error ξ_{tot}, (b) internal error ξ_{int}, (c) external error ξ_{ext}.

Obervations:

Fig.1 shows the behavior of the error figured obtained avaraging the errors associated to different configurations with $S = 100$ sparse multiple scatterers and for different signal to noise ratio ($SNR = 50dB$, $30dB$, $20dB$, $10dB$).

3 Preliminary Assessment

3.1 L-shaped Cylinders

Goal: show the performances of BCS when dealing with a sparse scatterer

- Number of Views: V
- Number of Measurements: M
- Number of Cells for the Inversion: N
- Number of Cells for the Direct solver: D
- Side of the investigation domain: L

Test Case Description

Direct solver:

- Square domain divided in $\sqrt{D} \times \sqrt{D}$ cells
- Domain side: $L = 3\lambda$
- $D = 1296$ (discretization for the direct solver: $< \lambda/10$)

Investigation domain:

- Square domain divided in $\sqrt{N} \times \sqrt{N}$ cells
- $L = 3\lambda$
- $2ka = 2 \times \frac{2\pi}{\lambda} \times \frac{L\sqrt{2}}{2} = 6\pi\sqrt{2} = 26.65$
- $\#DOF = \frac{(2ka)^2}{2} = \frac{(2 \times \frac{2\pi}{\lambda} \times \frac{L\sqrt{2}}{2})^2}{2} = 4\pi^2 \left(\frac{L}{\lambda}\right)^2 = 4\pi^2 \times 9 \approx 355.3$
- N scelto in modo da essere vicino a $\#DOF$: $N = 324$ (18×18)

Measurement domain:

- Measurement points taken on a circle of radius $\rho = 3\lambda$
- Full-aspect measurements
- $M \approx 2ka \rightarrow M = 27$

Sources:

- Plane waves
- $V \approx 2ka \rightarrow V = 27$
- Amplitude: $A = 1$
- Frequency: 300 MHz ($\lambda = 1$)

PEC Object:

- L-shaped cylinder

MT-BCS-based technique parameters:

- Gamma prior on noise variance parameter: $a = 5 \times 10^{-2}$
- Gamma prior on noise variance parameter: $b = 5 \times 10^{-2}$
- Convergenze parameter: $\tau = 1.0 \times 10^{-8}$
- Threshold: $\eta = 0.27$

Reconstruction profiles: 1 L-shaped Cylinder

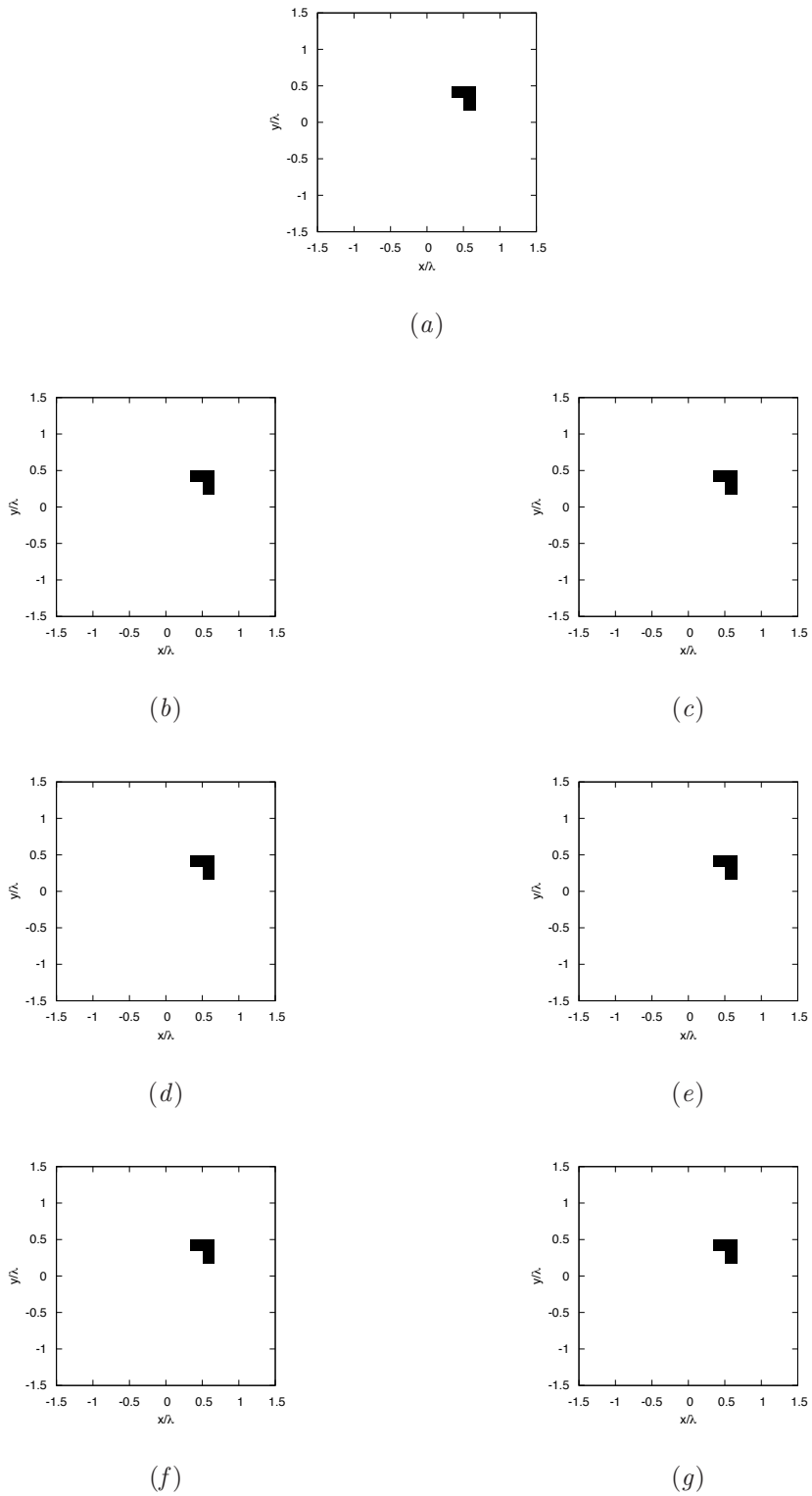

(a) (b) (c) (d) (e) (f) (g)

Figure 2. Actual object (a) and MT-BCS reconstructed object for $SNR = 50$ [dB] (b), $SNR = 40$ [dB] (c), $SNR = 30$ [dB] (d), $SNR = 20$ [dB] (e), $SNR = 10$ [dB] (f), and $SNR = 5$ [dB] (g).

Reconstruction profiles: 2 L-shaped Cylinders

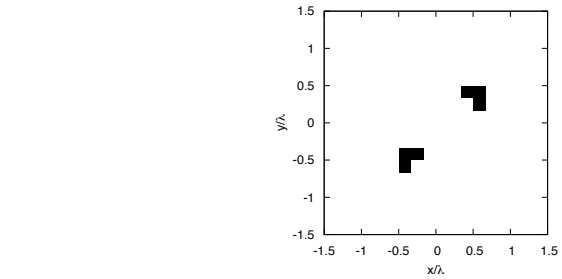

(a)

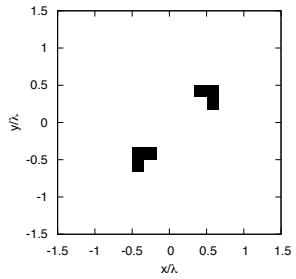

(b)

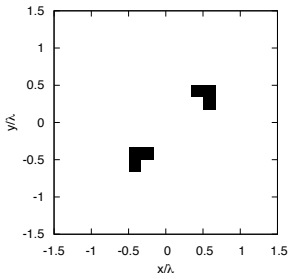

(c)

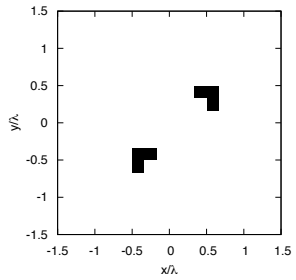

(d)

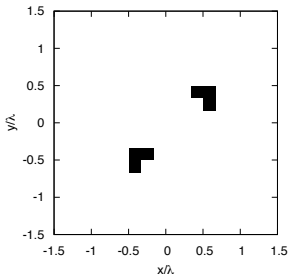

(e)

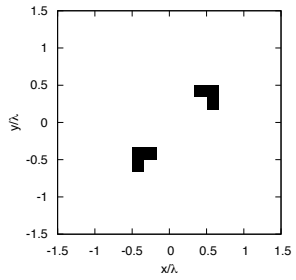

(f)

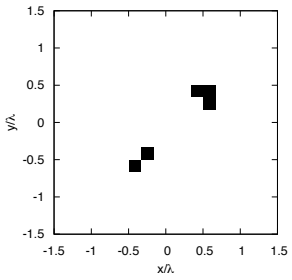

(g)

Figure 3. Actual object (a) and MT-BCS reconstructed object for $SNR = 50$ [dB] (b), $SNR = 40$ [dB] (c), $SNR = 30$ [dB] (d), $SNR = 20$ [dB] (e), $SNR = 10$ [dB] (f), and $SNR = 5$ [dB] (g).

Reconstruction profiles: 3 L-shaped Cylinders

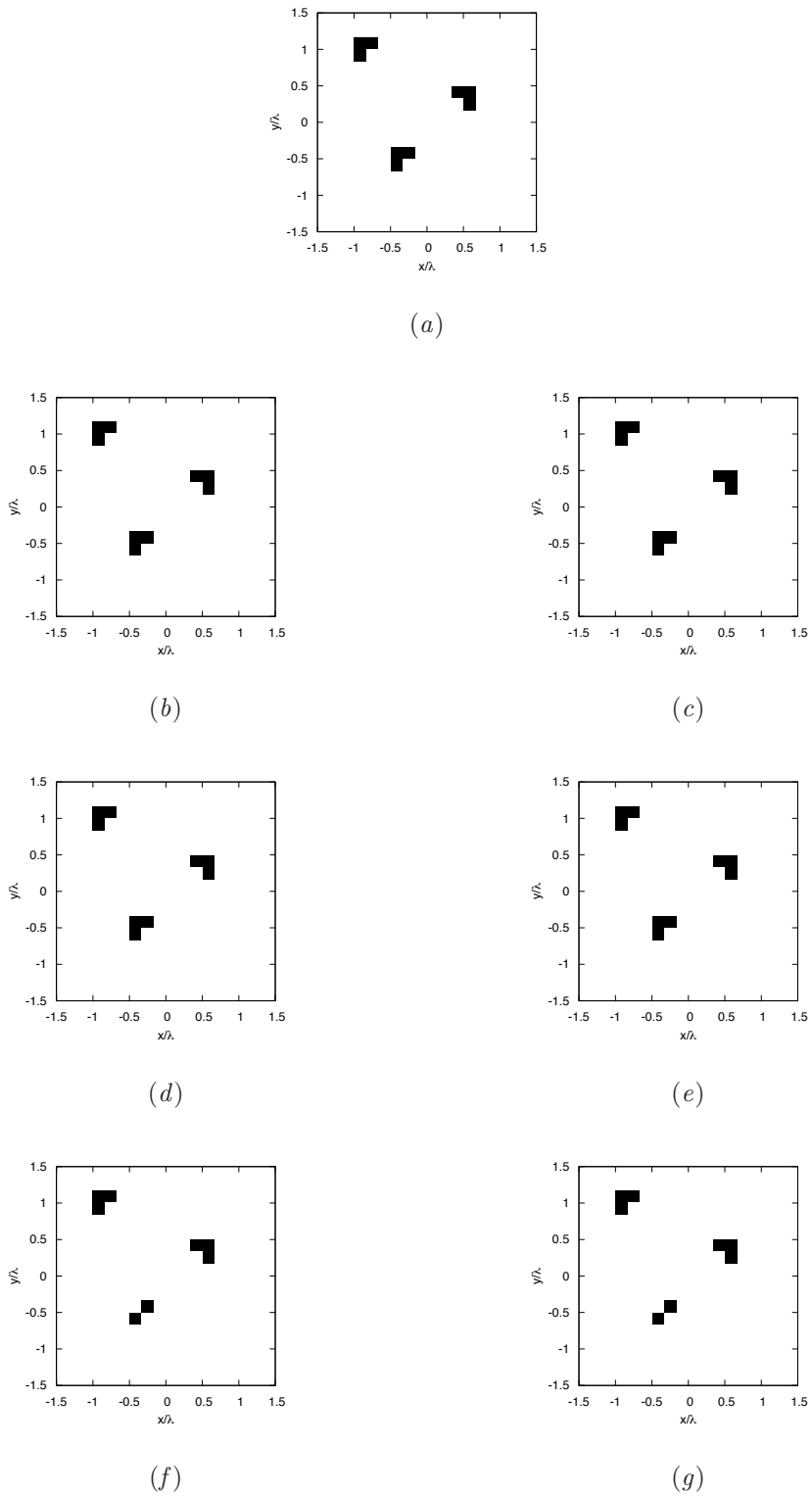

(a) (b) (c) (d) (e) (f) (g)

Figure 4. Actual object (a) and MT-BCS reconstructed object for $SNR = 50$ [dB] (b), $SNR = 40$ [dB] (c), $SNR = 30$ [dB] (d), $SNR = 20$ [dB] (e), $SNR = 10$ [dB] (f), and $SNR = 5$ [dB] (g).

Reconstruction profiles: 4 L-shaped Cylinders

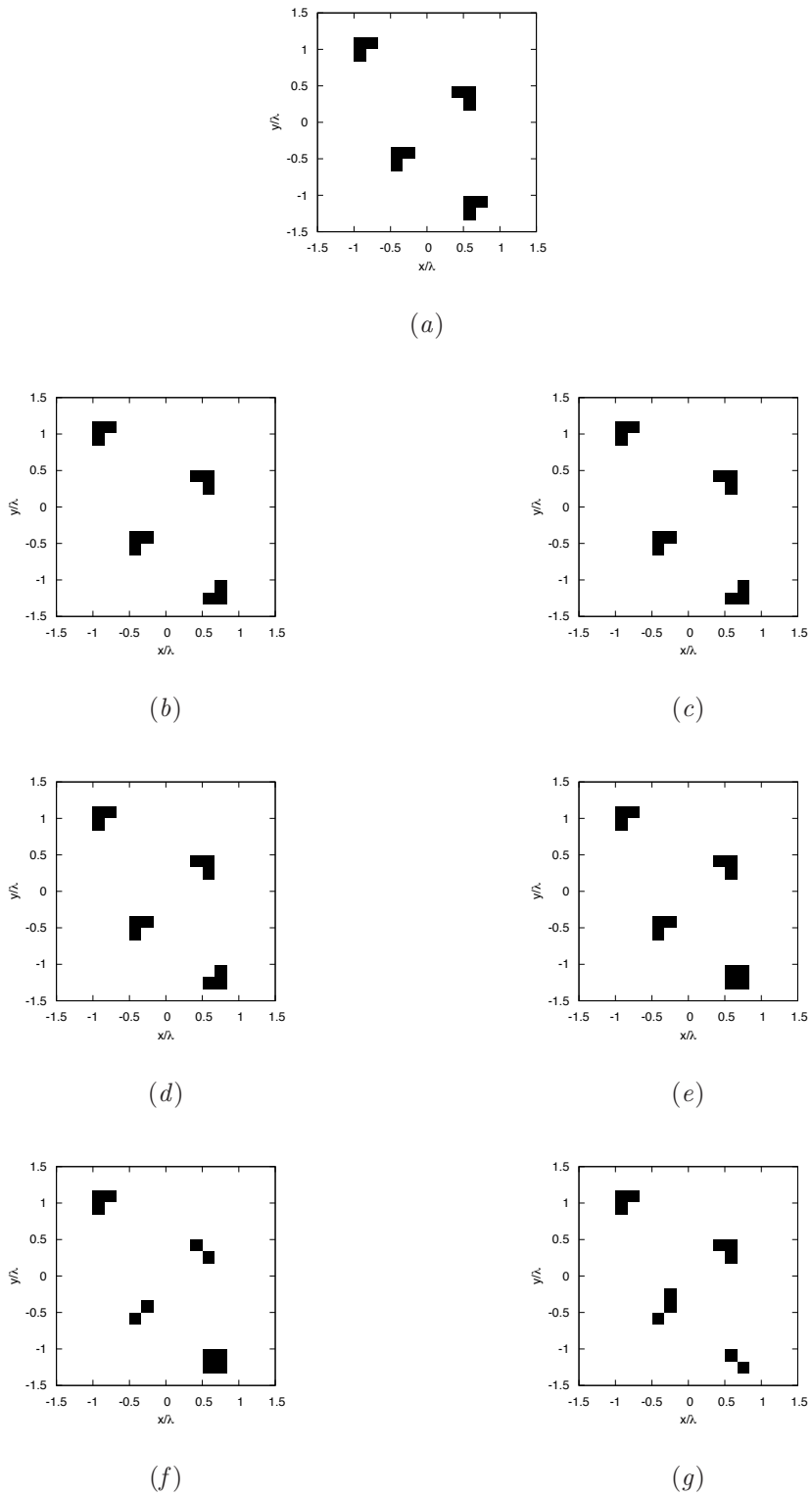

(a) (b) (c) (d) (e) (f) (g)

Figure 5. Actual object (a) and MT-BCS reconstructed object for $SNR = 50$ [dB] (b), $SNR = 40$ [dB] (c), $SNR = 30$ [dB] (d), $SNR = 20$ [dB] (e), $SNR = 10$ [dB] (f), and $SNR = 5$ [dB] (g).

$1\,L-shaped\,Cylinders$						
	$SNR=50\,dB$	$SNR=40\,dB$	$SNR=30\,dB$	$SNR=20\,dB$	$SNR=10\,dB$	$SNR=5\,dB$
ξ_{tot}	0.0	0.0	0.0	0.0	0.0	0.0
ξ_{int}	0.0	0.0	0.0	0.0	0.0	0.0
ξ_{ext}	0.0	0.0	0.0	0.0	0.0	0.0

$2\,L-shaped\,Cylinders$						
	$SNR=50\,dB$	$SNR=40\,dB$	$SNR=30\,dB$	$SNR=20\,dB$	$SNR=10\,dB$	$SNR=5\,dB$
ξ_{tot}	0.0	0.0	0.0	0.0	0.0	1.54×10^{-2}
ξ_{int}	0.0	0.0	0.0	0.0	0.0	0.25
ξ_{ext}	0.0	0.0	0.0	0.0	0.0	6.41×10^{-3}

$3\,L-shaped\,Cylinders$						
	$SNR=50\,dB$	$SNR=40\,dB$	$SNR=30\,dB$	$SNR=20\,dB$	$SNR=10\,dB$	$SNR=5\,dB$
ξ_{tot}	0.0	0.0	0.0	0.0	1.54×10^{-3}	1.54×10^{-3}
ξ_{int}	0.0	0.0	0.0	0.0	5.56×10^{-2}	5.56×10^{-2}
ξ_{ext}	0.0	0.0	0.0	0.0	0.0	0.0

$4\,L-shaped\,Cylinders$						
	$SNR=50\,dB$	$SNR=40\,dB$	$SNR=30\,dB$	$SNR=20\,dB$	$SNR=10\,dB$	$SNR=5\,dB$
ξ_{tot}	0.0	0.0	0.0	3.09×10^{-3}	9.26×10^{-3}	1.54×10^{-2}
ξ_{int}	0.0	0.0	0.0	0.0	0.17	0.25
ξ_{ext}	0.0	0.0	0.0	3.21×10^{-3}	3.21×10^{-3}	6.41×10^{-3}

Tab. I - Resume: ξ_{tot}, ξ_{int} and ξ_{ext} for different values of SNR [dB].

References

[1] L. Poli, G. Oliveri, and A. Massa, "Imaging sparse metallic cylinders through a Local Shape Function Bayesian Compressive Sensing approach," Journal of Optical Society of America A, vol. 30, no. 6, pp. 1261-1272, 2013.

[2] F. Viani, L. Poli, G. Oliveri, F. Robol, and A. Massa, "Sparse scatterers imaging through approximated multitask compressive sensing strategies," Microwave Opt. Technol. Lett., vol. 55, no. 7, pp. 1553-1558, Jul. 2013.

[3] L. Poli, G. Oliveri, P. Rocca, and A. Massa, "Bayesian compressive sensing approaches for the reconstruction of two-dimensional sparse scatterers under TE illumination," IEEE Trans. Geosci. Remote Sensing, vol. 51, no. 5, pp. 2920-2936, May. 2013.

[4] L. Poli, G. Oliveri, and A. Massa, "Microwave imaging within the first-order Born approximation by means of the contrast-field Bayesian compressive sensing," IEEE Trans. Antennas Propag., vol. 60, no. 6, pp. 2865-2879, Jun. 2012.

[5] G. Oliveri, P. Rocca, and A. Massa, "A bayesian compressive sampling-based inversion for imaging sparse scatterers," IEEE Trans. Geosci. Remote Sensing, vol. 49, no. 10, pp. 3993-4006, Oct. 2011.

[6] G. Oliveri, L. Poli, P. Rocca, and A. Massa, "Bayesian compressive optical imaging within the Rytov approximation," Optics Letters, vol. 37, no. 10, pp. 1760-1762, 2012.

[7] L. Poli, G. Oliveri, F. Viani, and A. Massa, "MT-BCS-based microwave imaging approach through minimum-norm current expansion," IEEE Trans. Antennas Propag., vol. 61, no. 9, pp. 4722-4732, Sept. 2013.

[8] G. Oliveri, N. Anselmi, and A. Massa, "Compressive sensing imaging of non-sparse 2D scatterers by a total-variation approach within the Born approximation," IEEE Trans. Antennas Propag., 2014, submitted.

[9] S. C. Hagness, E. C. Fear, and A. Massa, "Guest Editorial: Special Cluster on Microwave Medical Imaging," IEEE Antennas Wireless Propag. Lett., vol. 11, pp. 1592-1597, 2012.

[10] G. Oliveri, Y. Zhong, X. Chen, and A. Massa, "Multi-resolution subspace-based optimization method for inverse scattering," Journal of Optical Society of America A, vol. 28, no. 10, pp. 2057-2069, Oct. 2011.

[11] A. Randazzo, G. Oliveri, A. Massa, and M. Pastorino, "Electromagnetic inversion with the multiscaling inexact-Newton method - Experimental validation," Microwave Opt. Technol. Lett., vol. 53, no. 12, pp. 2834-2838, Dec. 2011.

[12] G. Oliveri, L. Lizzi, M. Pastorino, and A. Massa, "A nested multi-scaling inexact-Newton iterative approach for microwave imaging," IEEE Trans. Antennas Propag., vol. 60, no. 2, pp. 971-983, Feb. 2012.

[13] M. Salucci, D. Sartori, N. Anselmi, A. Randazzo, G. Oliveri, and A. Massa, "Imaging buried objects within the second-order Born approximation through a multiresolution-regularized inexact-Newton method", in 2013 International Symposium on Electromagnetic Theory (EMTS), Hiroshima, Japan, pp. 116-118, May 20-24, 2013.